



**Square supramolecular assemblies of uranyl complexes in organic solvents**

Journal:	<i>ChemComm</i>
Manuscript ID	CC-COM-07-2018-005277.R1
Article Type:	Communication

SCHOLARONE™  
Manuscripts



Cite this: DOI: 10.1039/xxxxxxxxxx

## Square supramolecular assemblies of uranyl complexes in organic solvents<sup>†</sup>

Michael J. Servis,<sup>a</sup> David T. Wu,<sup>\*b</sup> Jenifer C. Shafer,<sup>\*\*b</sup> and Aurora E. Clark,<sup>\*\*\*a</sup>

Received Date

Accepted Date

DOI: 10.1039/xxxxxxxxxx

www.rsc.org/journalname

**Uranyl nitrate/extractant complexes form long-range isotropic pairs and short-range ordered dimeric assemblies with a unique square configuration comprised of noncovalent ligand and acid anion mediated interactions, further stabilized by organic phase solvation.**

Supramolecular assembly of metal-ligand (ML) complexes is well documented in the synthetic inorganic chemistry literature and is known to be driven by the geometries of constituent interlocking complexes<sup>1,2</sup> that maximize noncovalent interactions (NCIs). The importance of more generalized “aggregation” phenomena of ML complexes is emerging in other domains, including separations science.<sup>3–7</sup> In the context of solvent extraction, one of the most significant processes is the Plutonium Uranium Reduction EXtraction Process (PUREX) used to recover uranium and plutonium from spent nuclear fuel.<sup>8,9</sup> There, the amphiphilic tributyl phosphate (TBP) extracts uranium as  $U(VI)O_2^{2+}$  with two nitrate anions from an acidic aqueous medium into an aliphatic organic solvent in the form  $UO_2(NO_3)_2(TBP)_2$ .<sup>10</sup> Yet, speciation may be more complex depending upon solution conditions, having a practical impact upon processing due to unwanted third phase formation, which is attributed to the aggregation of extracted ML species at high metal loading.<sup>11–14</sup> The structural and morphological features of those aggregates, informed by the fundamental driving forces behind their assembly, are yet to be understood. The degree of aggregation of the uranyl complexes affects their solubility in organic solutions, determining the metal loading limit before the onset of third phase formation. In this work, we consider the possibility of self-assembly of uranyl complexes using only the building blocks associated

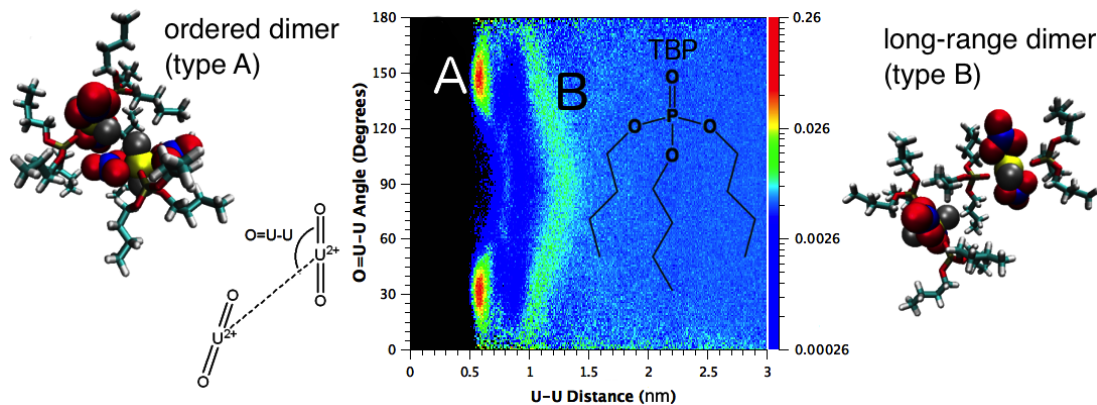
with the organic phase using classical molecular dynamics (CMD) augmented by cluster-based density functional theory (DFT) calculations and ab initio molecular dynamics (AIMD) simulations. These data demonstrate the occurrence of supramolecular assemblies of uranyl complexes in the organic phase, having well-defined square structural motifs whose formation is sensitive to extracting ligand structure and solvation environment.

Simulations of  $UO_2(NO_3)_2(L)_2$  complexes were conducted for combinations of extractant types and solvents (Tables 1 and S3). Three organophosphorus extractants were examined that probe the role of ligand alkyl tail length and head group structure: TBP, triamyl phosphate (TAP) and dibutyl butyl phosphonate (DBBP), illustrated in Figure S2. In the case of the TBP extractant simulations, both pure organic solvents and process-like conditions (where there is TBP in excess of the uranyl complexes and with coextracted water and nitric acid) were studied. The initial configurations of the organic phase simulations included preassembled  $UO_2(NO_3)_2(L)_2$  ( $L = \text{extractant}$ ) to avoid formation of metastable complexes persistent over the simulation time scale. Results were obtained from 250 ns of production time. Simulation system compositions, methodology and force field parameterization are discussed in the Supporting Information.

Self-association of the uranyl complexes is quantified by the  $U\dots U$  radial distribution function (RDF,  $g(r)$ ) with results for all CMD simulations provided in Figure S4. Importantly, the RDF peak positions are consistent across uranyl concentrations and solution conditions. This indicates the modes of association between complexes in *n*-dodecane and their general structural features at low concentration are representative of those found in systems up to the organic phase solubility limit. To isolate the pairwise interactions between uranyl complexes while still providing insight into the organization of the concentrated systems, the results are presented for 0.032 M solutions with concentration information presented in Supporting Information.

Figure 1 presents the pair distribution function  $g(r; \theta)$ , where  $r$  is the  $U\dots U$  distance and  $\theta$  is the  $O=U\dots U$  angle observed in *n*-dodecane with the TBP extractant. The four  $O=U\dots U$  angles

<sup>a</sup> Washington State University, Pullman WA.<sup>b</sup> Colorado School of Mines, Golden CO.<sup>\*</sup> E-mail: dwu@mines.edu<sup>\*\*</sup> E-mail: jshafer@mines.edu<sup>\*\*\*</sup> E-mail: auclark@wsu.edu<sup>†</sup> Electronic Supplementary Information (ESI) available. See DOI: 10.1039/b000000x/



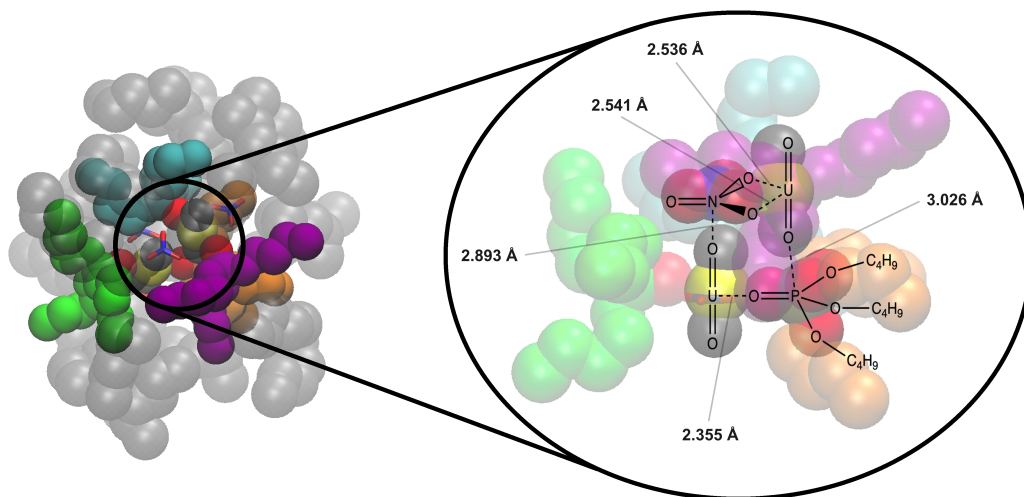
**Fig. 1** The pair distribution of uranium distances and O=U...U angles, averaged over the entire simulation production length of the equilibrated trajectories, is plotted for uranyl nitrate/TBP complexes in *n*-dodecane. Representative snapshots of the two primary uranyl interaction configurations are depicted, labeled A and B. Populations of each bin in  $r$  were normalized by a factor of  $4\pi r^2 \sin \theta$ . The bins were then normalized by the total number of counts at  $r$  for distances up to 30 Å.

exhibit symmetric distributions around 90°. Two predominant species corresponding to peaks in the pair distribution are observed: the first is an ordered dimer having a U...U distance near 6.0 Å and the second is a long-range uranyl pair having a correlation peak near 12.0 Å. The long-range uranyl pair is isotropic, associating through the polar cores but without a specific orientation of the uranyl ions. Interestingly, the 12.0 Å distance and isotropic organization of the long-range pair is conceptually similar to the hard spheres or ellipsoids that have been employed to model the experimental SAXS and SANS of process relevant solutions of uranyl, nitrate, and extractant.<sup>11,13–15</sup> In contrast to the long-range dimer, the ordered dimer exhibits directed interactions, illustrated by the distinct symmetric peaks in the pair distribution function for O=U...U angles centered at 30° and 150°. There, the -yl oxygen of one UO<sub>2</sub> is positioned in the cleft region between the equatorial ligands and the -yl oxygen of the second UO<sub>2</sub>. Although the equatorial ligands prevent a T-shaped coordination of the two UO<sub>2</sub> units<sup>16</sup>, the association is instead mediated by non-covalent ligand interactions. The total scattering profile for the systems herein, containing both the ordered and long-range dimers, exhibits very good agreement with the reported SAXS data (Figure S5). This indicates that the structures and relative concentrations of ordered and long-range dimers are consistent with experimental scattering data.

To further study the interactions, structure, and stability of the ordered supramolecular assembly, clusters consisting of the dimer with 24 solvating *n*-hexane were taken from the CMD trajectories and subjected to partial DFT geometry optimization followed by 100 fs of AIMD simulation. Four representative configurations were chosen having different angular orientations of the ligands and O=U...U angle (Figure S6 and Tables S4–S7). Given the high dimensionality of the cluster potential energy surface (PES) it is impractical to perform full DFT geometry optimization. Thus each structure was subjected to 50 optimization steps after which the gradient in energy achieved a value < -0.003 a.u. DFT calculations employed the M05-2X functional<sup>17</sup> with the Stuttgart basis set and small-core RECP for U-atoms,<sup>18</sup> the cc-pVDZ basis set<sup>19</sup> for N, O and P-atoms and the 6-31G\* basis set<sup>20</sup> for C- and H-

atoms chosen so as to keep double zeta quality while limiting the total number of basis functions to less than 4,500. The change in electronic energy upon formation of the ordered dimer was estimated to be -16.2 kcal/mol by the difference in energies between the DFT geometry of the uranyl dimer and that of the individual monomers, obtained from single point calculations without *n*-hexane solvent. Each cluster was observed to have an approximate square structural motif containing significant NCI of coordinating extractant and nitrate with UO<sub>2</sub> oxo-atoms, as shown in Figure 2. Of specific interest are the apical interaction of the phosphate P...O=U and the nitrate N...O=U. In the CMD, these are electrostatically attractive, as the P- and N-atoms have charges of 1.5955 and 0.75 e<sup>-</sup>, respectively, and the uranyl oxo-atom has a charge,  $q$ , of -0.45 e<sup>-</sup>. Relative to the initial CMD starting configuration, the partial DFT geometry optimization contracts the O<sub>U</sub>...P distance by 0.1–0.4 Å, indicating that the quantum mechanical treatment of the cluster fosters additional electrostatic interactions. The direction of the changes to the O<sub>U</sub>...N distance varied between dimers, but on average also contracted (Table S4 and S5). In comparison to a uranyl nitrate/TBP monomer with twelve solvating *n*-hexane, the Mulliken  $q$  on the U-atoms for the four dimer clusters was less positive, with changes between 0.03 and 0.2 e<sup>-</sup> (the exception being cluster 4 where one U-atom  $q$  increased by 0.03 e<sup>-</sup> and the other decreased by 0.36 e<sup>-</sup>).

Figure 2 presents the supramolecular assembly with DFT distances for cluster 1 while those geometric parameters for clusters 2–4 are in Supporting Information. Based upon the geometric changes to the DFT structure and the Mulliken  $q$ , the electrostatic interactions facilitated by the apical extractant and acid anion interactions with the uranyl oxo appear to be a significant contributor to dimer formation. These conclusions are further supported by AIMD simulation initiated from the DFT geometry of cluster 1 and performed for 100 fs, where the fluctuations in the local configurations were analyzed. The square structural motif persists throughout the AIMD trajectory, wherein the various interatomic distances may fluctuate by up to 0.4 Å with different periodicities over 100 fs. While the trajectory is relatively short, the complex remains stable during the trajectory with the U...U distance de-



**Fig. 2** Partially DFT optimized structure of an assembled  $\text{UO}_2(\text{NO}_3)_2(\text{TBP})_2$  dimer with solvating *n*-hexane molecules taken from the CMD simulation trajectory. TBP molecules are colored differently to highlight placement around the metal centers. Solvent molecules are shown in transparent gray for clarity. The structural motif and DFT distances of the square-shaped metal-ligand assembly is illustrated with a schematic overlay.

creasing slightly. The distances reported in Figure 2 are plotted as a function of time for the AIMD trajectory and provided in Figures S8 and S9.

Given the electrostatic stabilization of the square dimer, the choice of both anion and extractant are likely to influence the favorability of supramolecular assembly in solution. Steric interactions and the ability of the monomeric  $\text{UO}_2(\text{NO}_3)_2(\text{L})_2$  species to interlock with a second unit is also a contributing factor. To investigate this, the concentrations of both the ordered and long-range dimers have been measured as a function of the three extractants (Table 1). In addition to TBP, TAP and DBBP have been chosen to investigate the impact of increasing the extractant alkyl tail length (TAP) and removing a bridging phosphate ester oxygen (DBBP). Both influence the steric interactions of the monomer ML complex as well as solubility,<sup>12</sup> a topic of discussion in the next section. The concentration of the ordered dimers are determined by those U...U species having separation distances between 0 to 7.2 Å and the long-range isotropic dimers by distances between 7.2 to 13.6 Å with cut-off distances chosen from the RDF peak positions given in Figure S4. Changes to the extractant structure significantly impact the probability of forming both uranyl dimer types. The short-range ordered dimer is significantly reduced for DBBP compared to TBP. Removal of the electron withdrawing bridging oxygen reduces the positive charge of the phosphorus which in turn reduces the P...O=U electrostatic interaction. This does not affect the likelihood of observing the long-range dimer. Interestingly, the 12.0 Å correlation peak height is significantly reduced for TAP compared to TBP, indicating that alkyl tail steric overlap reduces formation of that type of dimer.

As demonstrated in Figure 3, the four TBPs position themselves into quadrants to avoid steric overlap of the alkyl tails. Considering the distribution between 0° and 180° of the six possible angles between pairs of the four TBP phosphorus atoms (see Supporting Information), the peak from oppositely facing TBP coordinated to the same  $\text{UO}_2$  occurs at 165° to 170°. There is a broad peak cen-

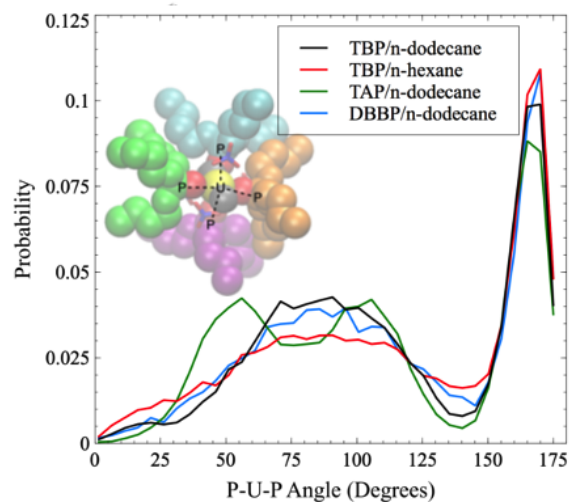


**Fig. 3** The distribution of angles between pairs of extractant ligands in assembled complexes (see inset) plotted for TBP, TAP and DBBP in *n*-dodecane and TBP in *n*-hexane.

tered around 90° from TBP molecules coordinated to the other  $\text{UO}_2$ . The inter-extractant angle distribution is similar for DBBP, however the five carbon tail length extractant, TAP, has a bimodal distribution for adjacent quadrants with peaks near 55° and 110°. This is the result of a steric interaction of the longer alkyl tail of TAP with a nitrate from the other  $\text{UO}_2$  complex, forcing the extractants to rotate slightly from the orthogonal orientation preferred by TBP. This may account for the modest reduction in ordered dimers for TAP compared to TBP. The combination of steric-based extractant orientation and the electrostatic driven square metal-ligand geometry demonstrates the multiple contributions associated with ligand structure to uranyl supramolecular assembly.

The final force that influences  $\text{UO}_2\cdots\text{UO}_2$  association is the or-

**Table 1** The total uranyl concentrations and number of short-range ordered dimers and long-range isotropic dimers per uranyl are given for each system. Process solvation environment corresponds to excess TBP and coextracted water and nitric acid for a 20% by volume TBP organic phase.

Extractant Type	Solvation Environment	Uranyl Conc. [mol/L]	Ordered Dimer per U	Isotropic Dimer per U
TBP	<i>n</i> -dodecane	0.032	0.10	0.253
DBBP	<i>n</i> -dodecane	0.032	0.012	0.239
TAP	<i>n</i> -dodecane	0.032	0.036	0.163
TBP	<i>n</i> -hexane	0.032	0.079	0.243
TBP	<i>n</i> -dodecane/process	0.032	0.031	0.197
TBP	<i>n</i> -hexane/process	0.032	0.014	0.145
TBP	toluene	0.032	0.006	0.119
TBP	<i>n</i> -dodecane/process	0.23	0.16	1.29

ganic phase solvation environment. In this case, the extracting ligands are known to have varying solubility and that in turn may alter the relative free energies of solvation of the supramolecular species. The concentration of each is presented in Table 1 as a function of organic solvent and the corresponding U...U RDFs are plotted in Figures S4 for TBP in *n*-dodecane and *n*-hexane, both as process-like and pure solvents, as well as pure toluene. Compared to *n*-dodecane solvent, *n*-hexane reduces the correlation peak near 6.0 Å without substantially impacting correlations at larger U...U distances. Within simulations having a process-like solution with *n*-dodecane and *n*-hexane, the ordered dimer at 6.0 Å is decreased, while the 12.0 Å long-range dimer is not as substantially impacted. The decrease in ordered dimer concentration in *n*-hexane compared to *n*-dodecane is consistent with the increased ML solubility limit for shorter chain length alkane solvents.<sup>21</sup> The shorter solvent chain length could more effectively overlap with and “wet” the extractant nonpolar tail region, which increases their solubility and reduces association in solution. Figure 3 also shows that the distribution of adjacent TBPs in the dimer which arrange into quadrants is broader for *n*-hexane compared to *n*-dodecane, indicating increased flexibility of the arrangement of extractants around the closely packed dimer for better wetting solvents. Lastly, in toluene uranyl association is most effectively suppressed, with *g*(*r*) values less than unity until becoming uncorrelated at U...U distances larger than 13.0 Å.

In conclusion,  $\text{UO}_2(\text{NO}_3)_2(\text{L})_2$  complexes form two dimeric species in organic solvents: long-range isotropic pairs and short-range ordered supramolecular assemblies that are stabilized by organic solvation, the ability of uranyl monomeric species to interlock, and electrostatic interactions via the ligand and acid anion. Nonpolar regions of the extractant exposed to the organic solvent arrange in a quadrant configuration while the linear uranyl dioxocations form a square assembly through direct electrostatic interaction with nitrate and phosphate ligands of the opposing uranyl. Extractant and solvent molecular structure directly affect the formation of the supramolecular assemblies. ML association is expected to be different for other classes of extractants, such as multidentate or acidic extractants, than for the family of solvating organophosphorus extractants considered in this study. These results, which identify the molecular scale interactions that enable association of uranyl nitrate/extractant complexes in organic solvents, may inform the design of extraction systems to control interactions between metal-ligand complexes to increase

metal solubility while inhibiting third phase formation.

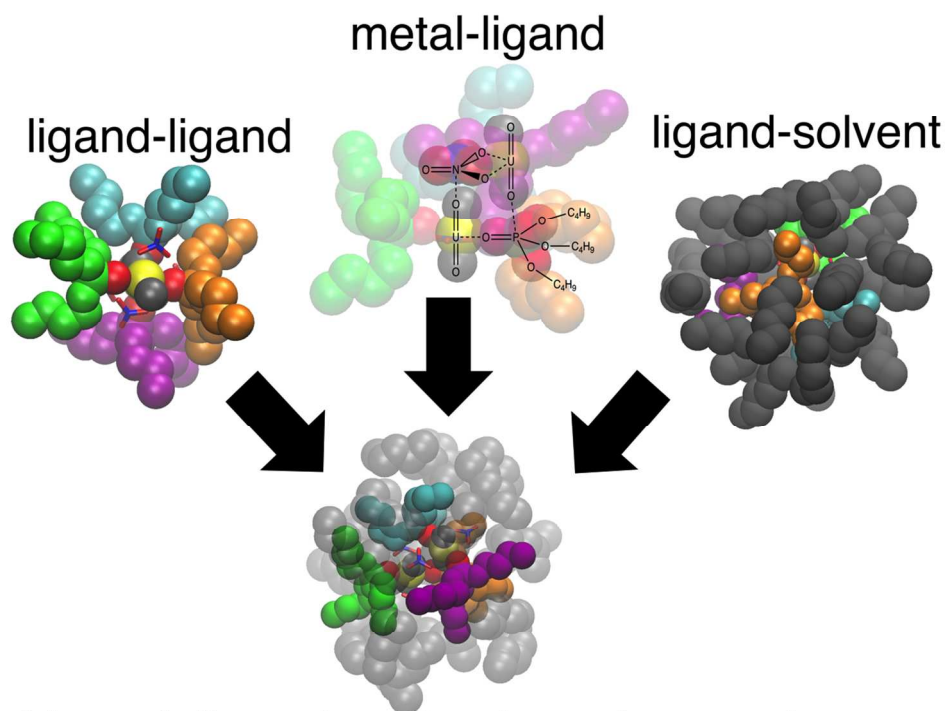
This work was supported by a grant from Department of Energy, Basic Energy Sciences Separations program (DE-SC0001815) and the Nuclear Regulatory Commission Faculty Development Award NRC-HQ-11-G-38-0062. This research used resources of Colorado School of Mines High Performance Computing center and the Oak Ridge Leadership Computing Facility located in the Oak Ridge National Laboratory, which is supported by the Office of Science within the Department of Energy under Contract No. DE-AC05-00OR22725.

## Conflicts of Interest

There are no conflicts to declare.

## References

- P. Wei, X. Yan and F. Huang, *Chemical Society Reviews*, 2015, **44**, 815–832.
- C. Brown, D. Toste, R. Bergman and K. Raymond, *Chemical Reviews*, 2015, **115**, 3012–3035.
- R. Ellis, Y. Meridiano, J. Muller, L. Berthon, P. Guilbaud, N. Zorz, M. Antonio, T. Demars and T. Zemb, *Chemistry: A European Journal*, 2014, **20**, 12796–12807.
- G. Ferru, D. Rodrigues, L. Berthon, O. Diat, P. Bauduin and P. Guilbaud, *Angewandte Chemie*, 2014, **53**, 5346–5350.
- M. Antonio, R. Ellis, S. Estes and M. Bera, *Physical Chemistry and Chemical Physics*, 2017, **19**, 21304–21316.
- D. Brigham, A. Ivanov, B. Moyer, L. Delmau, V. Bryantsev and R. Ellis, *Journal of the American Chemical Society*, 2017, **139**, 17350–17358.
- A. Baldwin, A. Ivanov, N. Williams, B. Ellis, R. ad Moyer, V. Bryantsev and J. Shafer, *ACS Central Science*, 2018.
- J. Rydberg, M. Cox, C. Musikas and G. Choppin, *Solvent Extraction Principles and Practices*, Marcel Dekker, New York, 2nd edn, 2004.
- K. Nash and J. Braley, *Advanced Separation Techniques for Nuclear Fuel Reprocessing Waste Treatment*, Woodhead Publishing Series in Energy, Cambridge, UK, 2011, pp. 3–22.
- K. Nash and G. Choppin, *Separation Science and Technology*, 1997, **34**, 255–274.
- R. Chiarizia, M. Jensen, M. Borkowski, J. Ferraro, P. Thiyagarajan and K. Littrell, *Solvent Extraction and Ion Exchange*, 2003, **21**, 1–27.
- P. Rao and Z. Kolarik, *Solvent Extraction and Ion Exchange*, 1996, **14**, 955–993.
- R. Chiarizia, M. Jensen, M. Borkowski, J. Ferraro, P. Thiyagarajan and K. Littrell, *Separation Science and Technology*, 2003, **38**, 3313–3331.
- R. Chiarizia, K. Nash, M. Jensen, P. Thiyagarajan and K. Littrell, *Langmuir*, 2003, **19**, 9592–9599.
- A. Baldwin, M. Servis, Y. Yang, N. Bridges, D. Wu and J. Shafer, *Journal of Molecular Liquids*, 2017, **246**, 225–235.
- P. Tecmer, S. Hong and K. Boguslawski, *Physical Chemistry and Chemical Physics*, 2016, **18**, 18305–18311.
- Y. Zhao, N. Schultz and D. Truhlar, *Journal of Chemical Theory and Computation*, 2006, **2**, 364–382.
- X. Cao and M. Dolg, *Journal of Molecular Structure: THEOCHEM*, 2004, **673**, 203–209.
- T. Dunning, *Journal of Chemical Physics*, 1989, **90**, 1007–1023.
- V. Rassolov, M. Ratner, J. Pople, P. Redfern and L. Curtiss, *Journal of Computational Chemistry*, 2001, **22**, 976–984.
- P. Rao, R. Dharmodaran, T. Srinivasan and C. Mathews, *Solvent Extraction and Ion Exchange*, 1993, **11**, 645–662.



Uranyl, ligand and solvent interactions lead to unique supramolecular assembly.

503x416mm (72 x 72 DPI)